Submitted to Appl. Surf. Sci. 3/25/2022

CO_2 Chemisorption and Dissociation on Flat and Stepped Transition Metal Surfaces

Wei Jin,[a, b *] Yingqi Wang,[b] Tong Liu,[a] Changchun Ding,[a] Hua Guo[b *]

[a] School of Science, Xihua University, Chengdu 610039, China

[b] Department of Chemistry and Chemical Biology, University of New Mexico, Albuquerque, NM 87113, USA

* Corresponding authors. E-mail: jinwei@mail.xhu.edu.cn (W. Jin) and hguo@unm.edu (H. Guo)

ABSTRACT

As a promising and practical way to decrease CO_2 emissions, the conversion of CO_2 to value-added chemicals has received significant recent attention. The activation of CO_2 on catalyst surfaces might proceed via a chemisorption state with a bent CO_2 configuration, in which substrate electrons are transferred into the antibonding orbital of the CO_2 adsorbate. Based on density functional theory calculations, we present an extensive survey of CO_2 chemisorption and dissociation on flat and stepped surfaces of several transition metals. The binding energy of the chemisorbed CO_2 is closely correlated with the extent of electron transfer from the metal to CO_2, as evidenced by a linear relationship found between the CO_2 adsorption energy and its Bader charge. Transition state scaling (TSS) correlations between binding energies of transition states and binding energies of either initial or final states are found to exist for the dissociation of the chemisorbed CO_2 on flat and stepped surfaces, which can be used to predict the efficacies of the catalysts. Our results show that defect sites at stepped surfaces have a strong influence on CO_2 chemical activation and dissociation.

Keywords: Chemisorbed CO_2, Dissociation, Stepped surfaces, DFT calculations

1. Introduction

Conversion of carbon dioxide (CO_2) molecules into valuable fuels and chemicals, such as carbon monoxide, methanol, ethanol, ethylene, and formic acids, has been proposed as a potential way to reduce the concentration of carbon dioxide in the atmosphere.[1] This carbon neutral strategy is an artificial scheme of carbon recycling to reduce the harm done by the consumption of fossil fuels.[2, 3] However, the current large-scale conversion of CO_2 remains a challenge and a great deal of research effort has been devoted to searching for effective means to activate CO_2. Among the various approaches explored, reduction of CO_2 to CO is often used as a model system in heterogeneous catalysis due to its simplicity and generality.[4] The related CO oxidation is also one of the most fundamental and important reactions in heterogeneous catalysis.[5]

The decisive step for CO_2 reduction is the activation of the rather stable CO_2 molecule by catalysts.[6, 7] Studies have shown that the interaction between the CO_2 molecule and transition metal surfaces is often weak physisorption where CO_2 typically assumes a linear configuration, suggesting little perturbation of the molecular electronic structure by the substrate.[8] However, it has also been observed that the CO_2 molecule can chemisorb on some transition metal surfaces, such as Ni,[9, 10] with a significantly bent structure.[8] Similar to the gas-phase CO_2^- anion which has a bent geometry,[11] the bent CO_2 adsorbate typically involves injection of fractional charge from the catalytic metal surface to the antibonding orbital of CO_2, thus activating the molecule. Importantly, chemisorbed CO_2 serves as a precursor of the CO_2 dissociation on some transition metal surfaces, such as Ni(100)[12] and Ni(110),[13, 14] according to the recent theoretical studies.[15-24] However, our understanding of chemisorbed CO_2 on other transition metal surfaces is quite limited. Thus, there is a need to gain a deeper understanding at the molecular level of the chemisorbed CO_2 and its dissociation in order to help design transition metal catalysts for CO_2 reduction.

It is well established that the surface structure of the catalyst has a significant impact on heterogeneously catalyzed processes.[5] CO_2 activation is no exception. Yang and coworkers studied CO_2 activation on Ni(111), Ni(100) and Ni(211) surfaces and found that the surface facets and defects have a profound influence on CO_2 activation.[25] Similar conclusions were reached on Cu surfaces.[26] Surface defects of the catalyst, particularly kinks and steps, are believed to form the active sites for adsorption and surface reaction processes.[27] Earlier experimental studies have revealed that CO_2 showed no chemisorption on defect free Cu single-crystal samples, such as the Cu(100)[28] or Cu(110)[29] surfaces. However, CO_2 molecules were found chemisorbed on the stepped Cu(332) surface.[30] Using DFT calculations, Muttaqien *et al*. found that CO_2 dissociation on Cu surfaces with step or kink defects has lower activation barriers than on the flat (111) surface.[20] Gustafson and coworkers reported that the presence of steps promotes CO_2 dissociation by lowering the dissociation barrier and reducing the CO and O recombination probability.[31] In a recent experimental study, CO_2 ejected from O and CO covered Pt surfaces is observed to have both thermal and hyperthermal channels,[32] and the thermal channel was shown to originate from trapping at the bent CO_2 chemisorption well.[33] Although CO_2 dissociation on low Miller index surfaces of a few transition metals was explored in previous work,[19, 34] the trends of CO_2 reduction on stepped surfaces with defect sites have not been carefully examined. Recent experimental studies using curved crystals have revealed important insights into facet-dependent surface chemistry,[35, 36] which challenges theoretical interpretation.

Herein, we performed DFT calculations to better understand CO_2 chemisorption on twenty-one transition metals, including both flat and stepped surfaces. The dissociation of CO_2 was further investigated if CO_2 chemisorption on the surface was detected. Reaction pathways for CO_2 dissociation on the stepped surfaces were examined in detail. These results allowed us to explore the scaling relationships between energies of the initial and transition states for CO_2

dissociation. These linear scaling relationships help to shed further light on the correlation between the chemisorption and activation of CO_2, which might be helpful for future design of new and more effective catalysts for CO_2 activation.

2. Computational methods and models

All calculations were performed using the spin-polarized density functional theory (DFT), as implemented in the Vienna Ab initio Simulation Package (VASP).[37, 38] The exchange-correlation energies were computed using the generalized gradient approximation functional of Perdew, Burke, and Ernzerhof (GGA-PBE).[39] While the valence electronic wave function was expanded in terms of plane waves with a ceiling (400 eV), the core electrons were approximated with the projector augmented wave (PAW) method.[40] The Brillouin zone integration was performed using *k*-point grids of 15×15×15 and 3×3×1 for bulk phase and supercell surface, respectively.[41] The convergence test and impact of dispersion correction can be found in the Supplementary Materials (SM). The structural optimization was carried out by a conjugate gradient algorithm until forces on all unconstrained atoms were below 0.05 eV/Å. The climbing image nudged elastic band method (CI-NEB) was employed to determine the transition state structure and the energy barrier.[42] Saddle points were considered converged when the maximum force in every degree of freedom was less than 0.05 eV/Å. Transition states were further verified through frequency calculations.

For the flat metal surfaces, the most stable facet of each transition metal surface was selected as follows: (111) for face centered cubic (FCC) metals (Ni, Cu, Rh, Pd, Ag, Ir, Pt and Au), (0001) for hexagonal centered cubic (HCP) metals (Co, Tc, Ru, Re and Os), and (110) for body centered cubic (BCC) metals (V, Cr, Fe, Nb, Mo, Ta and W). Three types of stepped surfaces, namely the (332) surface with (111) terraces, the (015) surface with (0001) terraces, and the (321) surface with (110) terraces, were chosen for FCC, HCP, and BCC transition metals, respectively. It should be mentioned that although Mn is conventionally considered as

a BCC metal, the Mn(321) surface was found to be unstable during optimization, thus the FCC structure of Mn was used instead. The flat and stepped surfaces of different transition metals selected are shown in Figure 1.

These metallic surfaces were all characterized using slab models. The flat surfaces were modeled by a four-layer slab, which contains a (3×3) unit cell, with the bottom layer fixed. The stepped surfaces were modeled with a (3×1) unit cell with three metal atoms per cell along the step edge. There were 24 atomic layers and the bottom six layers were fixed. A vacuum region of 15 Å was employed to avoid interaction in the z direction.

Adsorption energies were calculated according to the following equation:

$$E_{ads} = E_{adsorbate/slab} - E_{adsorbate} - E_{slab}$$

where $E_{adsorbate/slab}$, $E_{adsorbate}$ and E_{slab} are the energy of the adsorbed system, the isolated gas-phase molecule and the bare surface, respectively. A negative value of E_{ad} indicates that the adsorption is exothermic. Similarly, the transition-state energies E_{TS} relative to the gas-phase initial state were defined as:

$$E_{TS} = E_{TS/slab} - E_{gas\ CO_2} - E_{slab}$$

where $E_{TS/slab}$ and $E_{gas\ CO_2}$ correspond to the energy of the transition state (TS) system and the gas-phase CO_2 molecule, respectively. The difference between E_{TS} and E_{ads} gives the barrier for the dissociation of the chemisorbed CO_2.

The charge density difference (CDD) was described by the following expression:

$$\Delta\rho = \rho_{adsorbate/slab} - \rho_{slab} - \rho_{adsorbate}$$

where $\rho_{adsorbate/slab}$ ρ_{slab} and $\rho_{adsorbate}$ represent the charge density of the adsorbed systems, the bare surface and the isolated gas-phase molecule, respectively.

3. Results and Discussion

3.1 CO_2 chemisorption on flat surfaces

As mentioned earlier, CO_2 has two possible adsorption configurations on transition metal surfaces, namely physisorption and chemisorption. The physisorbed state features a linear CO_2* configuration, while the chemisorbed one corresponds to a bent configuration. To investigate the activation of CO_2, we first determined the most stable initial state (IS) for CO_2 chemisorption on flat surfaces of all selected transition metals. The CO_2*/Pt(111), CO_2*/W(110), and CO_2*/Ru(0001) structures were chosen to illustrate the chemisorption of CO_2 on different flat surfaces. For these three exemplary cases, the optimized configurations of chemisorbed CO_2* on different flat surfaces are given on the left-hand side of Figure 2.

For FCC(111) surfaces, the coinage metal surfaces (Cu(111), Ag(111), and Au(111)) do not support chemisorbed CO_2*, consistent with previous theoretical and experimental studies.[20, 43] On other (111) surfaces, the chemisorbed CO_2* preferentially occupies the bridge site in a bidentate form with the C atom and one O atom anchored on two adjacent metal atoms, resulting in both C-Metal and O-Metal bond lengths of ~2.1 Å. The most favorable configuration of chemisorbed CO_2* on BCC(110) flat surfaces is somewhat different. The CO_2* adsorbate often forms a tridentate configuration, occupying a long bridge (LB) site with two O atoms at two neighboring bridge sites. On HCP(0001) surfaces, CO_2* also preferentially takes a tridentate adsorption configuration, occupying a hollow (H) site with the C atom and two O atoms binding to three transition metal atoms. Besides, the calculated adsorption energies of chemisorbed CO_2* on some close-packed flat surfaces are compared with previous results in Table S2 in SM.

The calculated adsorption energy and total Bader charge of the chemisorbed CO_2* on various flat surfaces are summarized in yellow squares in Figure 1. From the left to the right of the periodic table, the binding of chemisorbed CO_2* gradually weakens, which is consistent with the decrease in the number of transferred charges of the corresponding metals. The charge transfer from the metal surface to CO_2 is estimated by Bader charges to analyze the degree of

activation for chemisorbed CO_2* on transition metal surfaces. As shown by the data in the Figure 1, significant electron transfer from the metal to the chemisorbed molecule is apparent, which is clearly responsible for the bent geometry of the adsorbate due to the partial filling of the antibonding orbital. The more charge the metal transfers to CO_2, the stronger the interaction between the metal surface and CO_2. In Cu, Ag and Au metals, the *d* orbitals are fully filled and the *s* orbital is half-filled. These stable electron configurations make the electron transfer to CO_2* rather difficult, thereby preventing CO_2 chemisorption.

For these systems, a linear relationship is found between CO_2* adsorption energy and its Bader charge, shown in Figure 3a, presenting strong evidence in support of the notion that the strength of CO_2* chemisorption is correlated with electron transfer. We also note that some of the adsorption energy is positive, indicating that the chemisorption is meta-stable. In other words, there is a barrier that separates the chemisorption and physisorption wells, as demonstrated by recent calculations of global potential energy surfaces.[21-24] The relationship between adsorption energies of chemisorbed CO_2* on flat transition metal surfaces and electronegativity of these metals is also explored and the results are plotted in Figure S2 in SM. For transition metals in the same row, there is a linear relationship between their electronegativities and adsorption energies. Taking 3d metals as an example, it can be seen that the lower the electronegativity, the stronger the interaction between the metal surface and CO_2.

3.2 CO_2 chemisorption on stepped surfaces

As expected, there are more possible adsorption sites for CO_2* on stepped surfaces. Two sites were selected in this work to investigate the CO_2* chemisorption and dissociation. One is the edge site where CO_2* is parallel to the step edge, and the other is the step site where CO_2* is perpendicular to the step edge. The CO_2*/Pt(332), CO_2*/W(321), and CO_2*/Ru(015) systems were chosen to exemplify the FCC(332), BCC(321) and HCP(015) stepped surfaces, respectively.

The bent CO_2* chemisorbed at the edge site on the FCC(332), BCC(321) and HCP(015) surfaces are shown in the left-hand side of Figure 4. On FCC(332) edge sites, the chemisorbed CO_2* adapts a bidentate configuration, occupying a bridge (B) site with C atom and one O atom binding to two neighboring metal atoms along the edge. The calculated adsorption energy and Bader charge of chemisorbed CO_2* at the edge site on stepped surfaces are summarized in the green squares in Figure 1. We did not find a chemisorbed state of CO_2* on Ag(332) and Au(332) due to the weak interaction with these stepped surfaces. However, there is a chemisorption state for CO_2* on Cu(332) with a bent configuration, although the adsorption is quite weak. On the BCC(321) and HCP(015) edge sites, the chemisorbed CO_2* are both tridentate, much like their adsorption states on the corresponding flat surfaces. As on flat surfaces, the adsorption energy of the chemisorbed CO_2* on steps also weakens gradually from left to the right of the periodic table. Similarly, there is also significant charge transfer from the metal to the adsorbate, leading to the occupation of the CO_2* antibonding orbital and hence the bent structure. Early transition metals tend to transfer more charge to the CO_2* adsorbate than the late transition metals. There is also a clear linear scaling relationship between the adsorption energy of chemisorbed CO_2* and the Bader charge, as shown in Figure 3b. The more electrons transferred from the surface to CO_2*, the stronger the binding is. Ta is an outlier and its deviation from the linear scaling is discussed in SI.

Comparing with the edge site, the configurations of chemisorbed CO_2* at the step site are more diverse. The left-hand side of Figure 5 shows the configurations of chemisorbed CO_2* at the step site on different stepped surfaces. For the CO_2*/FCC(332) system, CO_2 chemisorbs with a bidentate configuration at the S1 site with one O atom binding to a metal atom at the edge of the step and the C atom binding to a metal atom at lower terrace. Again, the only coinage metal that can support chemisorbed CO_2* is Cu, but the adsorption energy is quite small. For the CO_2*/BCC(321) system, CO_2 chemisorbs with a tridentate configuration at the

S2 site, where one O atom is adsorbed on a bridge site at the edge, the other O atom binds to a metal atom in the lower terrace, and C atom is anchored on a top site at the terrace. For the CO_2*/HCP(015) system, CO_2 chemisorbs with a tridentate configuration at the S3 site, where one O atom binds to a metal atom at the step edge, while the C atom and the other O atom bind to two adjacent metal atoms in the lower terrace, respectively. The calculated adsorption energy of the chemisorbed CO_2* at the step site on the stepped surfaces are summarized in the blue squares in Figure 1. Again chemisorbed CO_2* was not found at step sites of Ag(332) and Au(332) surfaces. As shown in Figure 3c, the Bader charge also has a linear relationship with the adsorption energy of chemisorbed CO_2* at step sites, where Ta is again an outlier (see discussion in SI). The range of the negative charge of the chemisorbed CO_2* decreases from -1.72|e| to -0.39|e|, which also corresponds to decreasing adsorption energies.

The comparison of the adsorption energies of CO_2* chemisorbed on the terrace, edge, and step sites of different transition metal surfaces is shown in Figure 6. These transition metals were divided into BCC, HCP and FCC groups according to the most stable structure to ensure that the transition metals in the same group have the similar flat and stepped surfaces. Although CO_2* chemisorption is meta-stable (with positive adsorption energies) at terrace sites for most FCC and HCP metal surfaces, BCC metals display a much stronger ability to capture CO_2 at terrace sites. The results implied that more open surfaces have stronger interactions with the CO_2* adsorbate. In addition, it can be clearly seen that stepped surfaces also have stronger interaction with CO_2* than flat surfaces. This is especially clear for Cu, where chemisorbed state of CO_2 is not available on the (111) flat surface, but available on the (332) stepped surface. This is apparently due to the lower coordination of the step and edge metal atoms of stepped surfaces, leading to the higher reactivity of these metal atoms.[33, 44] For the CO_2*/FCC metal systems, it is found that the CO_2* chemisorbed at the edge site is preferred over the step sites on stepped surfaces, based on calculated adsorption energies. This preference was also found

for HCP metals, but the binding energies of the chemisorbed CO_2* at edge and step sites are much closer. However, for the CO_2*/BCC metal systems, the step site on the stepped surface becomes the preferred site, except for W and Ta.

The CO_2*/Ru(0001) structure was chosen to analyze the interaction of CO_2 with the metal surfaces, in order to identify the activated state of the CO_2 molecule. Figure 7 provides insights into the interaction mechanism of CO_2 with Ru(0001), which is divided into two steps. The first step is to bend the CO_2 molecule in the gas phase, while the second step is the binding of the bent CO_2 with the Ru(0001) surface. The DOS of the free CO_2 gas molecule with the linear and bent configurations are shown in Figure 7a and 7b, respectively. The free bent CO_2 was optimized with the angle fixed at the same value adopted in the adsorbed configuration. For a free CO_2 molecule with a linear configuration (Figure 7a), the highest occupied molecular orbital (HOMO) is the degenerate $1\pi_g$ bonding orbitals, while the lowest unoccupied molecular orbital (LUMO) is the degenerate $2\pi_u$ antibonding orbitals, which is consistent with other studies.[43, 45] When the O=C=O skeleton changes from a linear to bent (C_{2v}) configuration (Figure 7b), the $1\pi_g$ ($2\pi_u$) orbitals split into the $1a_2$ and $4b_2$ ($6a_1$ and $2b_1$) orbitals. As a result, the newly formed $6a_1$ orbital becomes the LUMO, and the $4b_2$ orbital becomes the HOMO. When the bent CO_2 approaches and binds to the Ru(0001) surface, the antibonding $6a_1$ orbital of the chemisorbed CO_2* shifts below the Fermi level and mixes with 4d orbital of Ru atoms, as shown in Figure 7c. This is similar to what has been observed for CO_2 adsorption on the Au (211) surface in the presence of a Na^+ ion solvated in a water bilayer.[46] The charge density difference (CDD) for chemisorbed CO_2* on Ru(0001) surface was also explored and the results are plotted in Figure 7c, where the yellow and cyan regions represent the accumulation and the depletion of electrons, respectively. It can be seen that the electrons are transferred from the surface Ru atoms to the chemisorbed CO_2. The accumulation (yellow region) of charge density around the Ru-C bonds reflects the strong covalent interaction, which also confirms CO_2

chemisorption on the Ru(0001) surface. Figure 7d shows the projected DOS of surface Ru atoms bound to the adsorbed molecule in Figure 7c. Comparing Figure 7c and 7d, it can be seen that the projected DOS of surface Ru atoms does not change significantly before and after CO_2 chemisorption. Similar behaviors have been found for CO_2 chemisorption on other metal surfaces.[17] The LDOS of chemisorbed CO_2* on Pt, W, and Ru surfaces are displayed in Figure 8, while those of others are collected in the SM (Figures S3-S5). Except for chemisorbed CO_2* on the Pt surface, all of orbital energies of the chemisorbed CO_2* shift below the Fermi level, indicating stronger interaction between the chemisorbed CO_2* and the metal surfaces. It can also be used to explain the trend observed in Figure 1 that the adsorption energy of CO_2* on Pt surface is weaker than that on W and Ru surfaces.

3.3 CO_2 dissociation on flat surfaces

Now we investigate the dissociation of the chemisorbed CO_2* into CO* and O* on flat surfaces. Figure 2 displays the initial state (IS), transition state (TS), and final state (FS) along the dissociation pathway on three exemplary flat surfaces. The adsorption configuration and corresponding adsorption energy of the chemisorbed CO_2* on different flat surfaces, which serve as the IS (the left panels) in the NEB calculations, have been described in Section 3.1.

Based on numerous previous calculations on transition metal surfaces, O* atom prefers to adsorb at a hollow site, i.e., the fcc site for FCC(111) surfaces and the hcp site for BCC(110) and HCP(0001) surfaces, while the top site is in general more favorable for CO*.[47-49] Hence, we chose in this study the same FS, in which CO* is adsorbed vertically at a top site with its C atom binding with one metal atom and O* is stably adsorbed at a hollow site (marked with top-h), as shown in the right-hand side of Figure 2. Then transition states were searched by the CI-NEB method, as described in Sec. 2. The TS for dissociation on the Pt (111), W(110), and Ru(0001) flat surfaces are depicted in the middle panels of Figure 2. CO_2 dissociation on the Pt (111) surface starts with chemisorbed CO_2* at B site. At the TS, the OC-O bond breaks and

O atom migrates from the hollow site to a nearby bridge site. The OC-O distance is elongated from 1.30 to 1.98 Å with CO nearly perpendicular to the surface. The reaction pathway of CO_2 dissociation on the Pt (111) surface is marked as B→top-h, where B represents the adsorption site of the reactant, the symbols "top" and "h" denote the products CO* and O* are adsorbed respectively at top and hollow sites, with CO perpendicular to the surface. Similar notations are used for the reaction pathways of CO_2* dissociation on different surfaces discussed below. On the W(110) surface, the dissociation starts with a tridentate CO_2* and reaches TS when the spectator CO moiety rotates to break its O-metal bond, while the O atom migrates from the bridge site to a nearby bridge site. During this process, the OC-O distance is elongated from 1.38 to 1.72 Å. Finally, the FS features CO* at the top site perpendicular to the surface and O* at the hollow site. For CO_2 dissociation on the Ru(0001) surface, the bidentate CO_2* at the IS breaks the OC-O bond with CO* and O* moving apart. The OC-O distance is elongated from 1.24 Å at IS to 1.70 Å at TS. Further separation between the two leads to the FS where CO* adsorbed at the top site perpendicular to the surface, and O* at hollow site.

3.4 CO_2 dissociation on stepped surfaces

Stepped surfaces with different step facets were constructed to gain insight into the impact of defect sites on dissociation of CO_2*. Two types of reaction pathways were investigated, one along the edge and the other along the step, similar to those reported in previous studies.[20, 44] Pt(332), W(321) and Ru(015) structures were used as exemplars for FCC(332), BCC(321) and HCP(015) stepped surfaces, respectively. The corresponding reaction paths along and perpendicular to the step edge are shown in Figures 4 and 5, respectively. The adsorption configurations and corresponding adsorption energies of the chemisorbed CO_2* on the Pt(332), W(321) and Ru(015) stepped surfaces, which serve as the ISs (the left panels), have been described in Section 3.2. The FSs, i.e., the dissociated CO* and O* species with most stable adsorption sites and structures, are different as shown in the right panels of Figure 4. CO* was

found to adsorb most strongly at a top or bridge (b) site, and O is more likely to occupy a bridge (b) or hollow (h) site.

Along the Pt-edge, the dissociation starts with the chemisorbed CO_2* as a reactant adsorbed at the bridge (B) site. As the OC-O bond breaks, CO and O moves apart along the edge of the stepped surface to form the TS. The OC-O distance is elongated from 1.29 to 2.03 Å. The reaction proceeds further leading to the FS, where CO* and O* are adsorbed at top and hollow sites (marked as top-h), respectively. For the dissociation along W-edge, the dissociation starts with the bent CO_2* adsorbed at the B site and ends with CO* and O* co-adsorbed at two bridge sites (b-b). The elongated C-O band length of TS is only 1.46 Å on W-edge. At Ru-edge, reaction pathway is marked as B→top-b. Starting from the reactant (bent CO_2*) adsorbed at the B site, the OC-O bond is elongated to 1.64 Å at TS. Then CO and O continue to move apart, and finally form the FS where CO* is located vertically at a top site and O* is located at a bridge site.

Similar analyses were carried out for the dissociation along the step of stepped surfaces. As shown in Figure 5, the reaction pathway along the Pt-step is marked as S1→top-h. Starting with the chemisorbed CO_2* initially at the S1 site as IS, the OC−O bond elongates to form TS where the OC-O distance changes from 1.29 to 2.11 Å. It finally ends with CO* adsorbed on a top site in lower terrace and O* adsorbed on a hollow site at the edge (top-h). Along the W-step, the reaction pathway is S2→b-b. From IS to TS, the OC-O distance is elongated from 1.39 to 1.63 Å. For CO_2* dissociation on the Ru-step, the IS features a bent CO_2* adsorbed at the S3 site. At TS, the OC-O bond is elongated to 1.82 Å. A similar FS was observed on the Ru-step, only O* is adsorbed at upper step edge while CO* is adsorbed in lower step terrace. It can be seen that the elongated C−O bond lengths of TSs are also dependent on the type of transition metal and surface geometry.

From the results summarized in Figure 1, it is clear that there are many transition metal surfaces that support chemisorption of CO_2, characterized by large negative adsorption energies. Furthermore, these surfaces with strongly adsorbed CO_2 also correlate to low dissociation barriers, which is more quantitatively discussed in the next section. This is very encouraging as these metals could potentially provide catalytic activities for CO_2 activation.

3.5 Transition-state scaling relations

It has been widely demonstrated that linear energy relationships, including scaling relationships for adsorption energies and the Brønsted−Evans−Polanyi (BEP) relationships for activation energies, provide insightful understanding of the catalytic performance of transition metals.[19, 50] The transition-state scaling (TSS) correlation is an alternative form of the BEP relationship originally proposed by Alcala et al., which can be cast in terms of the initial, final, and transition state energies.[51] Two possible correlation types, i.e., initial state TSS and final state TSS correlations, were plotted in Figure 9 for the dissociation of chemisorbed CO_2* on various transition metal surfaces.

As shown in Figure 9a-c, the TS energies for CO_2* dissociation on the flat, edge and step sites are found to scale linearly with the adsorption energies of the chemisorbed CO_2 (marked as E_{ad}(bent-CO_2)). Comparing Figure 9a and 9b, the slope of scaling relationship on the stepped surfaces is almost the same as the corresponding slope on flat surfaces, while the difference in the intercept is 0.61 eV. This big difference reflects the geometrical effect of the step sites for CO_2* dissociation compared to the flat surfaces.[27] The fitted linear equations on the edge and step of stepped surfaces are very similar, as shown in Figure 9b and 9c. The slopes for CO_2* dissociation on edge and step sites of stepped surfaces are 1.05 and 1.13, respectively, where the difference of the intercept is only 0.19 eV. A similar scaling relationship exists between the TS energies E_{TS} and the FS energies E_{FS}, as shown in Figure 9d-f. It can be seen that CO_2 dissociation shows excellent linear scaling relations, that is, the higher the energy of

IS or FS, the higher the dissociation barrier. Generally, the initial state TSS correlation is better than the final state TSS correlation. This is understandable since the reactant, namely chemisorbed CO_2*, has similar geometries on the different surfaces, while the co-adsorption configurations of the CO* and O* are more complicated and have more possible combinations. Even for the same type of surfaces, the most stable configuration of CO* and O* varies substantially from metal to metal. For initial state or final state TSS correlations, the linear relation for the terrace site is better than those for the edge and step sites. This can be explained by the simplicity of flat surfaces, which results in fewer choices of the adsorption configurations for IS, TS and FS, making the correction more obvious.

Although the overall linear scaling relationship is promising, there are some exceptions that deviate substantially from the linear scaling. As shown in Figure 9a, Pt(111) and Pd(111) are two outliers whose TS energies are much higher than those assumed by the relationship, although they have similar TS structures with other FCC metals. The adsorption energy of the chemisorbed CO_2* on the Pt(111) surface was calculated to be 0.38 eV, which is consistent with previously reported values of 0.39 eV and 0.38 eV.[32, 33] Besides, the TS energy (1.31 eV) on Pt(111) surface agrees well with the value of 1.37 eV reported by Deng et al.[33] Similarly, the chemisorption energy of CO_2 on the Pd (111) surface is also in line with Deng et al.'s work.[33] It is also worth mentioning that both the TS geometries on Pt(111) and Pd(111) surfaces reported in this work are very close to those in studies mentioned above . Comparing the OC-O distance at TS on different flat surfaces, it is found that when the elongated C−O bond length is no longer than 1.8 Å, the TS energy fits well into the scaling relation. While the elongated C−O bond lengths at TS is 2.0 Å on Pt(111) and 1.9 Å on Pd(111) surfaces, both of which exceed 1.8 Å, suggesting extremely "late" barriers. Besides, the standard DFT calculations underestimate the preference of CO* for low-coordination binding sites on the Pt(111) surface which is known as the "CO/Pt(111) puzzle".[52, 53] It may be one more reason

why Pt deviates from the linear relationship. The linear scaling relation at the edge site of stepped surfaces holds well for most metals except Pd, as shown in Figure 9b. The barrier on the Pd(332) surface is also found to be very "late", with a C-O distance of 2.2 Å, far exceeding that of other metals. To summarize, Pd and Pt are somewhat different from other transition metals due to the fact that they have a "late" TS that is much closer to the FS which leads to a higher TS energy.

4. Conclusions

In this work, the chemisorption and dissociation of CO_2 on the flat and stepped surfaces of twenty-one transition metals were surveyed using plane-wave DFT. We found that CO_2 chemisorbs on most transition metals with a bent configuration, expect for coinage metals (Cu, Ag, and Au) where the chemisorption does not exist except for stepped surfaces. Charge calculations confirmed significant electron transfer from metals to the CO_2 adsorbate, suggesting the bent configuration of the adsorbate is due to injection of metal electrons into the antibonding orbital of the adsorbate. Indeed, a linear relationship between the CO_2 adsorption energy and its Bader charge is found: the more charge transferred from the metal surface to the CO_2 moiety, the more strongly the CO_2 binds to the surface.

Two additional linear correlations, i.e., the initial state TSS and final state TSS correlations were found as an alternative form of BEP relation. The scaling relationships can be used to predict the effectiveness of catalysts for similar chemical reactions. Our results suggest that the chemisorption of CO_2 and its dissociation are greatly affected by electronic structure of the transition metals, which controls the binding strength of chemisorbed CO_2 by how much charge transferred from the surface to the CO_2 moiety. In addition, our results suggest that the CO_2 binding strength and activation barrier of transition metal catalysts are significantly enhanced at defect sites, such as steps on the surfaces. This trend suggests strategies for designing novel catalysts that are more effective in activating CO_2.

Perhaps most importantly, our calculations identified a number of transition metal surfaces that provide strong chemisorption for CO_2. Furthermore, the strongly bound CO_2 on these surfaces are also associated with lower dissociation barriers, particularly at defect sites. These new discoveries indicate they can potentially be used to activate this stable molecule.

Acknowledgements:

This work was financially supported by the Scientific Research Foundation of Xihua University (Grant No. RZ2000002854 to J. W.) and by National Science Foundation (Grant. No. CHE-1951328 to H. G.). We thank the Key Laboratory of Advanced Scientific Computation of Xihua University and the Center for Advanced Research Computing (CARC) at the University of New Mexico for high-performance computing services.

Figure captions:

Figure 1: Summary of the calculated adsorption energy (eV) and Bader charge (|e|) of the bent CO_2* chemisorbed on flat and stepped surfaces of various transition metals. The color of the boxes denotes the adsorption sites: yellow for terrace sites on flat surfaces, green and blue for edge and step sites on stepped surfaces.

Figure 2: Stationary point geometries (top and side views) along the reaction pathway of CO_2* dissociation on the flat surfaces of Pt, W, and Ru. From left to right: the initial state (IS), transition state (TS), and final state (FS). The carbon and oxygen atoms are shown as dark brown and red balls, respectively.

Figure 3: Linear scaling relationship between the adsorption energy and the transferred charge for chemisorbed CO_2* on (a) the terrace site on flat surfaces, (b) the edge, and (c) step sites of stepped surfaces.

Figure 4: Stationary point geometries (top and side views) along the reaction pathway of the CO_2* dissociation on the edge site of the stepped surfaces of Pt, W, and Ru. From left to right: initial state (IS), transition state (TS), and final state (FS). The carbon and oxygen atoms are shown as dark brown and red balls, respectively.

Figure 5: Stationary point geometries (top and side views) along the reaction pathway of the CO_2* dissociation on the step site of stepped surfaces of Pt, W, and Ru. From left to right: initial state (IS), transition state (TS), and final state (FS). The carbon and oxygen atoms are shown as dark brown and red balls, respectively.

Figure 6: Comparison of CO_2* chemisorption energies on different sites of different transition metals.

Figure 7: Interaction mechanism of CO_2 with the Ru(0001) surface. Density of states (DOS) of the free CO_2 with the (a) linear and (b) bent configurations, respectively. The DOS for Ru(0001) (c) with and (d) without CO_2* adsorbed. The charge density difference (CDD) for CO_2* chemisorbed on Ru(0001) surface is also given in (c). The yellow (cyan) region represents charge accumulation (depletion). The dashed line indicates the Fermi level.

Figure 8: Local density of states (LDOS) for CO_2* chemisorbed on transition metal surfaces. (a)-(c) LDOS for the Pt(111), W(110) and Ru(0001) flat surfaces. (d)-(f) LDOS for the edge site of step surfaces of Pt, W, and Ru. (g)-(i) LDOS for the step site of step surfaces of Pt, W, and Ru. The dashed line indicates the Fermi level.

Figure 9: Scaling relationship for CO_2* dissociation on different transition metal surfaces. Calculated transition-state energies for bent CO_2 dissociation as a function of CO_2* adsorption energies on (a) flat surfaces, (b) edge and (c) step of stepped surfaces. Calculated transition-state energies for CO_2* dissociation as a function of the sum of CO* and O* adsorption energies on (d) flat surfaces, (e) edge and (f) step of stepped surfaces.

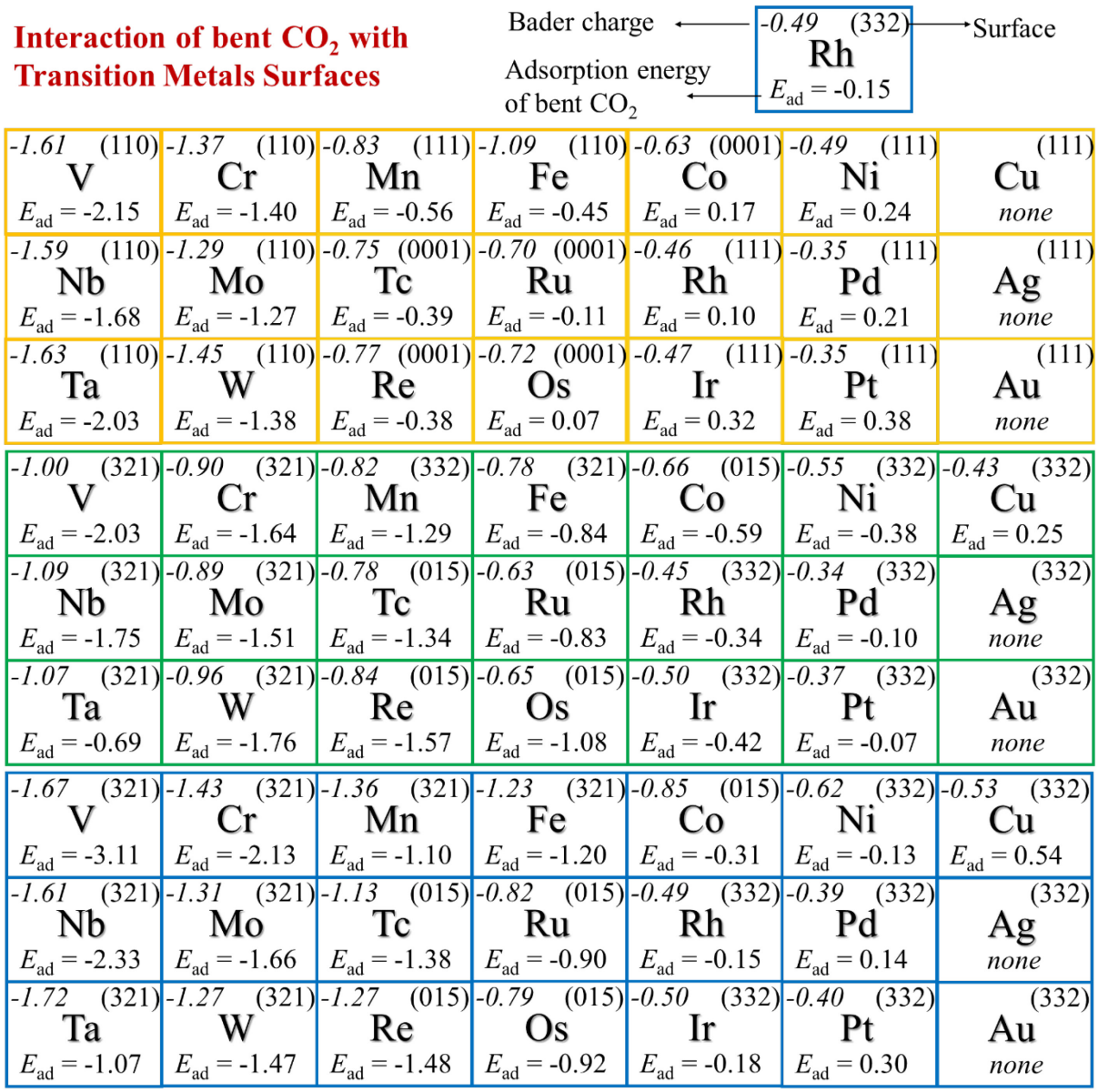

W. Jin et al. Figure 1

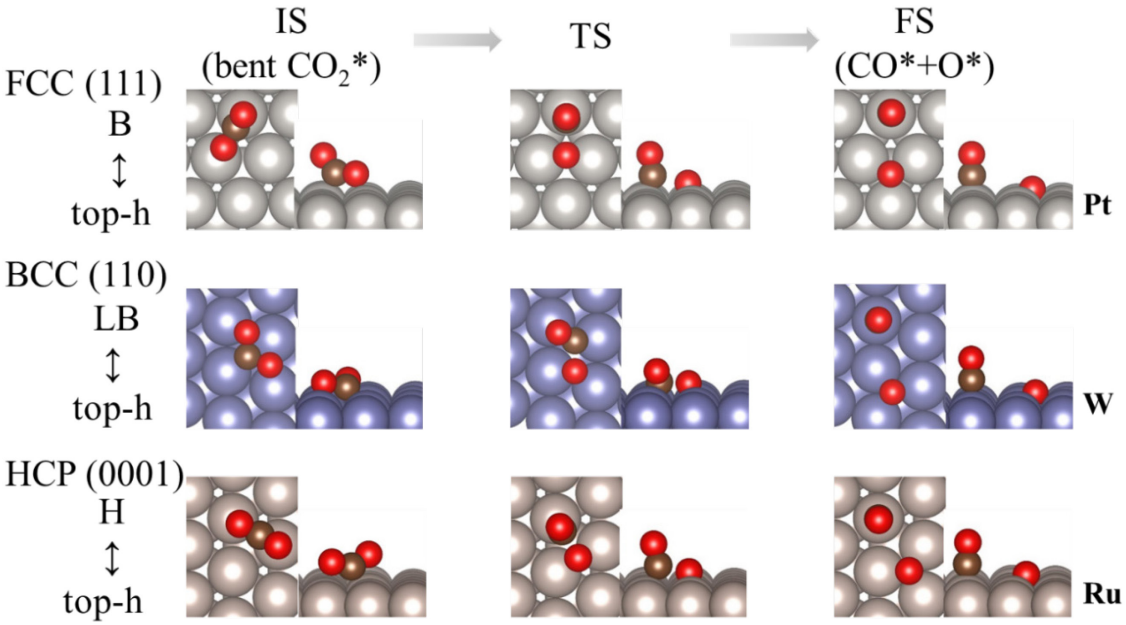

W. Jin et al. Figure 2

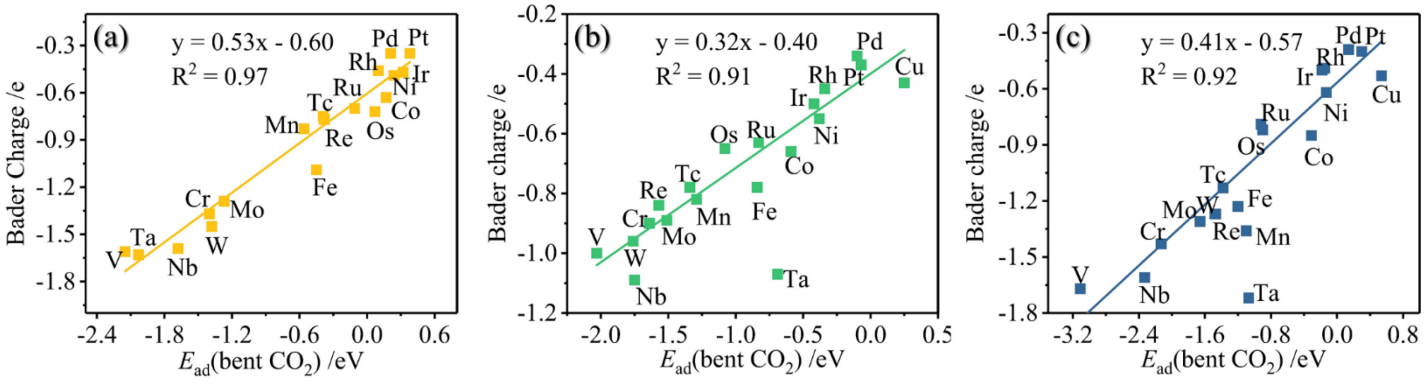

W. Jin et al. Figure 3

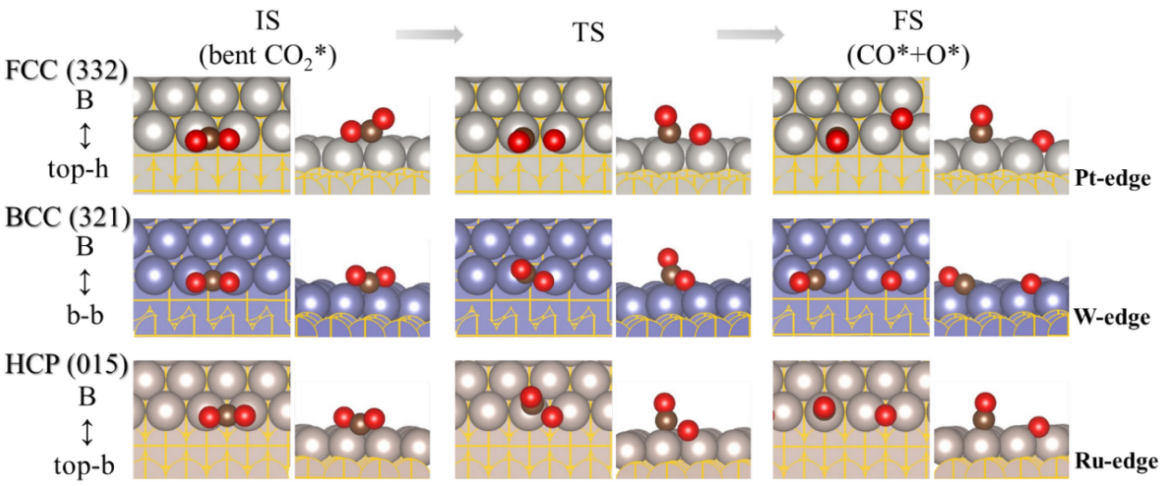

W. Jin et al. Figure 4

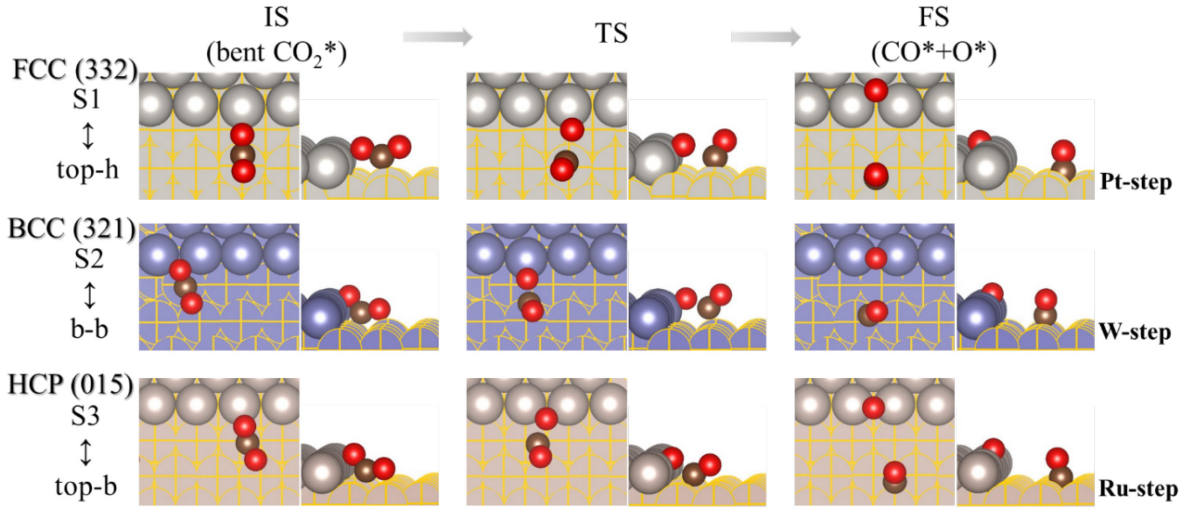

W. Jin et al. Figure 5

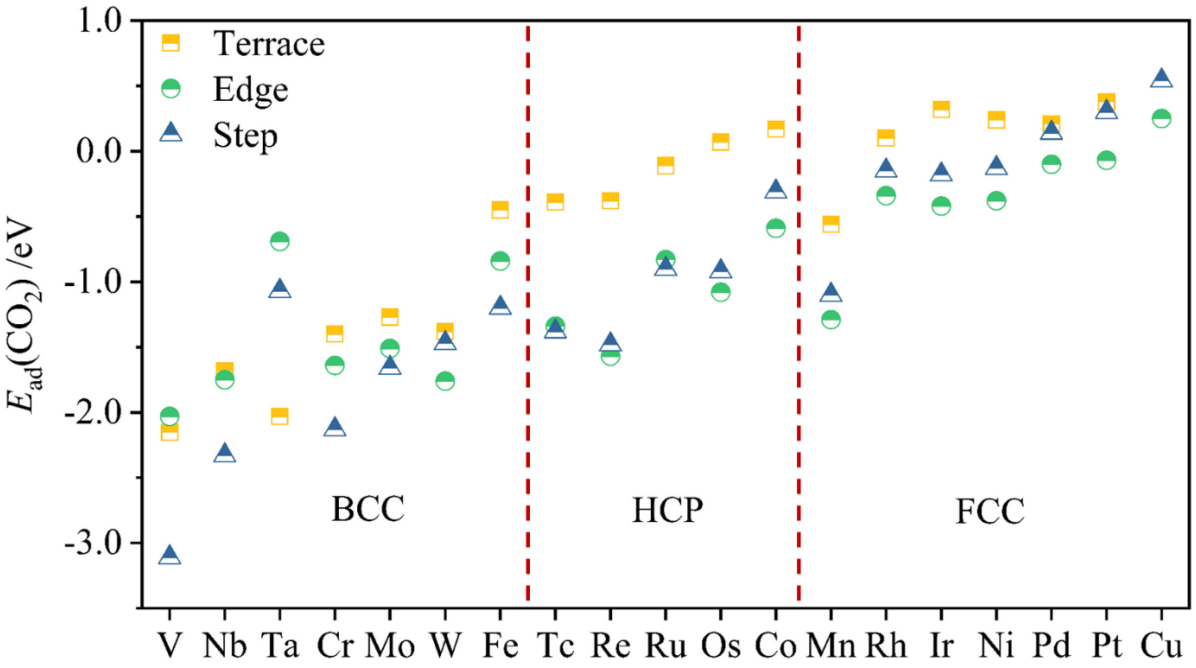

W. Jin et al. Figure 6

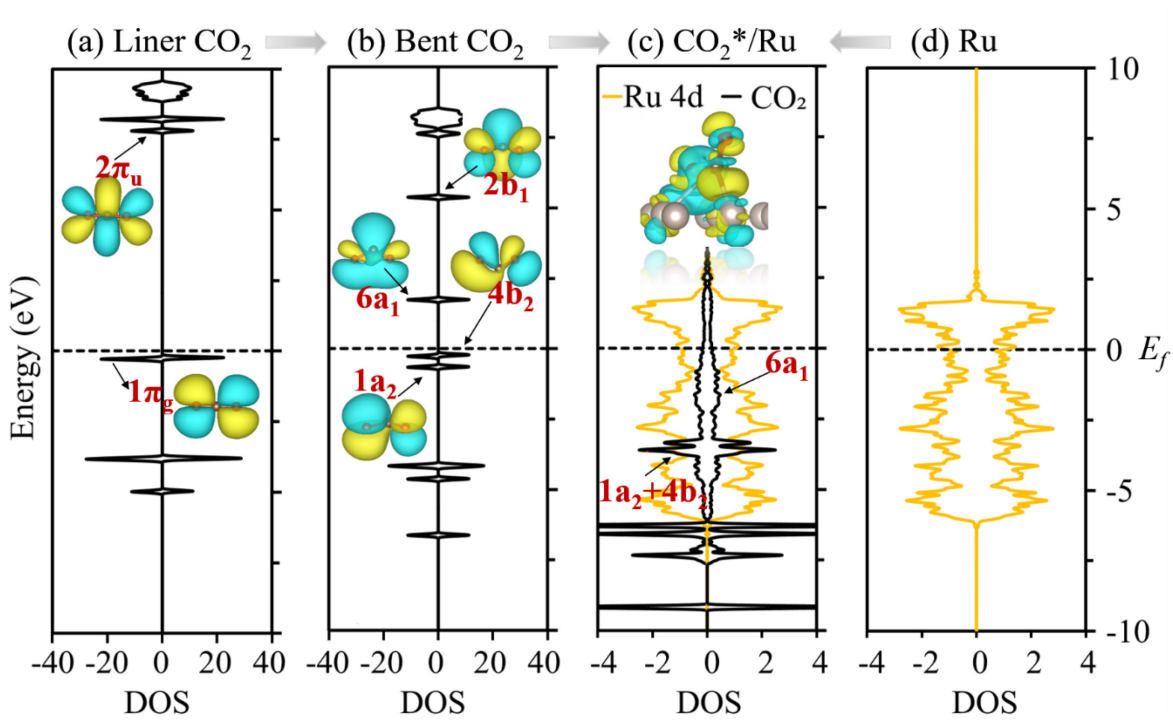

W. Jin et al. Figure 7

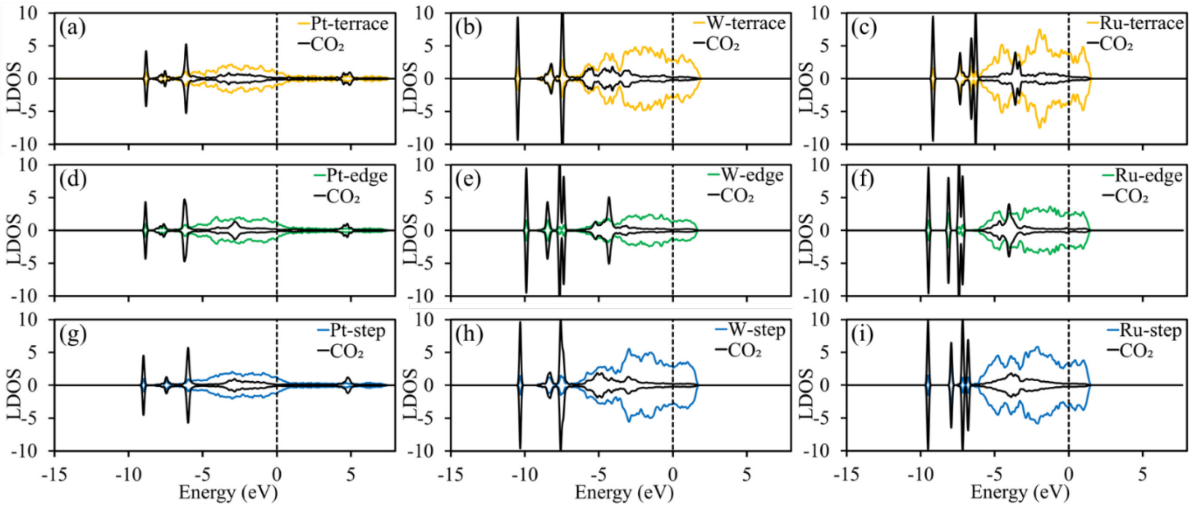

W. Jin et al. Figure 8

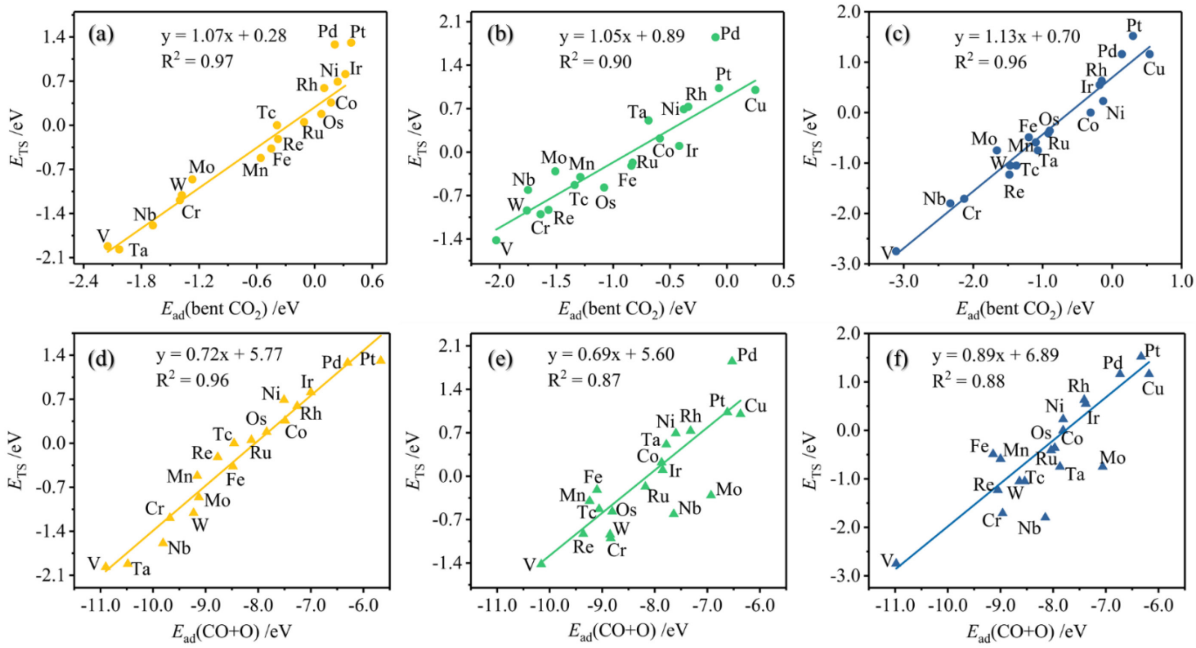

W. Jin et al. Figure 9

References:

[1] R.S. Haszeldine, Carbon capture and storage: How green can black be?, Science, 325 (2009) 1647-1652.
[2] H. Arakawa, M. Aresta, J.N. Armor, M.A. Barteau, E.J. Beckman, A.T. Bell, J.E. Bercaw, C. Creutz, E. Dinjus, D.A. Dixon, K. Domen, D.L. DuBois, J. Eckert, E. Fujita, D.H. Gibson, W.A. Goddard, D.W. Goodman, J. Keller, G.J. Kubas, H.H. Kung, J.E. Lyons, L.E. Manzer, T.J. Marks, K. Morokuma, K.M. Nicholas, R. Periana, L. Que, J. Rostrup-Nielson, W.M.H. Sachtler, L.D. Schmidt, A. Sen, G.A. Somorjai, P.C. Stair, B.R. Stults, W. Tumas, Catalysis research of relevance to carbon management: Progress, challenges, and opportunities, Chem. Rev., 101 (2001) 953-996.
[3] A.Y. Khodakov, W. Chu, P. Fongarland, Advances in the development of novel cobalt Fischer−Tropsch catalysts for synthesis of long-chain hydrocarbons and clean fuels, Chem. Rev., 107 (2007) 1692-1744.
[4] S. Nitopi, E. Bertheussen, S.B. Scott, X. Liu, A.K. Engstfeld, S. Horch, B. Seger, I.E.L. Stephens, K. Chan, C. Hahn, J.K. Nørskov, T.F. Jaramillo, I. Chorkendorff, Progress and perspectives of electrochemical CO_2 reduction on copper in aqueous electrolyte, Chem. Rev., 119 (2019) 7610-7672.
[5] G.A. Somorjai, Introduction to Surface Chemistry and Catalysis, Wiley, New York, 1994.
[6] H.J. Freund, R.P. Messmer, On the bonding and reactivity of CO_2 on metal surfaces, Surf. Sci., 172 (1986) 1-30.
[7] U. Burghaus, Surface chemistry of CO_2 – Adsorption of carbon dioxide on clean surfaces at ultrahigh vacuum, Prog. Surf. Sci., 89 (2014) 161-217.
[8] H.J. Freund, M.W. Roberts, Surface chemistry of carbon dioxide, Surf. Sci. Rep., 25 (1996) 225-273.
[9] X. Ding, L. De Rogatis, E. Vesselli, A. Baraldi, G. Comelli, R. Rosei, L. Savio, L. Vattuone, M. Rocca, P. Fornasiero, F. Ancilotto, A. Baldereschi, M. Peressi, Interaction of carbon dioxide with Ni(110): A combined experimental and theoretical study, Phys. Rev. B, 76 (2007) 195425.
[10] C. Dri, A. Peronio, E. Vesselli, C. Africh, M. Rizzi, A. Baldereschi, M. Peressi, G. Comelli, Imaging and characterization of activated CO_2 species on Ni(110), Phys. Rev. B, 82 (2010) 165403.
[11] J. Pacansky, U. Wahlgren, P.S. Bagus, SCF ab-initio ground state energy surfaces for CO_2 and CO_2^-, J. Chem. Phys., 62 (1975) 2740-2744.
[12] M.P. D'Evelyn, A.V. Hamza, G.E. Gdowski, R.J. Madix, Dynamics of the dissociative adsorption of CO_2 on Ni(100), Surf. Sci., 167 (1986) 451-473.
[13] B. Bartos, H.J. Freund, H. Kuhlenbeck, M. Neumann, H. Lindner, K. Müller, Adsorption and reaction of CO_2 and CO_2/O CO-adsorption on Ni(110): Angle resolved photoemission (ARUPS) and electron energy loss (HREELS) studies, Surf. Sci., 179 (1987) 59-89.
[14] J. Wambach, G. Illing, H.J. Freund, CO_2 activation and reaction with hydrogen on Ni(110): formate formation, Chem. Phys. Lett., 184 (1991) 239-244.
[15] S.J. Choe, H.J. Kang, D.H. Park, D.S. Huh, J. Park, Adsorption and dissociation reaction of carbon dioxide on Ni(1 1 1) surface: molecular orbital study, Appl. Surf. Sci., 181 (2001) 265-276.
[16] S.-G. Wang, D.-B. Cao, Y.-W. Li, J. Wang, H. Jiao, Chemisorption of CO_2 on nickel surfaces, J. Phys. Chem. B, 109 (2005) 18956-18963.
[17] S.-G. Wang, X.-Y. Liao, D.-B. Cao, C.-F. Huo, Y.-W. Li, J. Wang, H. Jiao, Factors controlling the interaction of CO_2 with transition metal surfaces, J. Phys. Chem. C, 111 (2007) 16934-16940.
[18] D.B. Cao, Y.W. Li, J.G. Wang, H.J. Jiao, CO_2 dissociation on Ni(211), Surf. Sci., 603 (2009) 2991-2998.

[19] C. Liu, T.R. Cundari, A.K. Wilson, CO_2 reduction on transition metal (Fe, Co, Ni, and Cu) surfaces: In comparison with homogeneous catalysis, J. Phys. Chem. C, 116 (2012) 5681-5688.
[20] F. Muttaqien, Y. Hamamoto, K. Inagaki, Y. Morikawa, Dissociative adsorption of CO_2 on flat, stepped, and kinked Cu surfaces, J. Chem. Phys., 141 (2014) 034702.
[21] B. Jiang, H. Guo, Communication: Enhanced dissociative chemisorption of CO_2 via vibrational excitation, J. Chem. Phys., 144 (2016) 091101.
[22] X. Zhou, B. Kolb, X. Luo, H. Guo, B. Jiang, Ab Initio molecular dynamics study of dissociative chemisorption and scattering of CO_2 on Ni(100): Reactivity, energy transfer, steering dynamics, and lattice effects, J. Phys. Chem. C, 121 (2017) 5594-5602.
[23] A. Farjamnia, B. Jackson, The dissociative chemisorption of CO_2 on Ni(100): A quantum dynamics study, J. Chem. Phys., 146 (2017) 074704.
[24] M. del Cueto, X. Zhou, L. Zhou, Y. Zhang, B. Jiang, H. Guo, New perspectives on CO_2–Pt(111) interaction with a high-dimensional neural network potential energy surface, J. Phys. Chem. C, 124 (2020) 5174-5181.
[25] J. Cai, Y. Han, S. Chen, E.J. Crumlin, B. Yang, Y. Li, Z. Liu, CO_2 activation on Ni(111) and Ni(100) surfaces in the presence of H_2O: An ambient-pressure X-ray photoelectron spectroscopy study, J. Phys. Chem. C, 123 (2019) 12176-12182.
[26] T. Yang, T. Gu, Y. Han, W. Wang, Y. Yu, Y. Zang, H. Zhang, B. Mao, Y. Li, B. Yang, Z. Liu, Surface orientation and pressure dependence of CO_2 activation on Cu surfaces, J. Phys. Chem. C, 124 (2020) 27511-27518.
[27] J.K. Nørskov, T. Bligaard, B. Hvolbæk, F. Abild-Pedersen, I. Chorkendorff, C.H. Christensen, The nature of the active site in heterogeneous metal catalysis, Chem. Soc. Rev., 37 (2008) 2163-2171.
[28] P.A. Taylor, P.B. Rasmussen, I. Chorkendorff, Carbon dioxide chemistry on Cu(100), J. Vac. Sci. Technol. A, 10 (1992) 2570-2575.
[29] S.S. Fu, G.A. Somorjai, Interactions of O_2, CO, CO_2, and D_2 with the stepped Cu(311) crystal face: Comparison to Cu(110), Surf. Sci., 262 (1992) 68-76.
[30] I.A. Bönicke, W. Kirstein, F. Thieme, A study on CO_2 dissociation on a stepped (332) copper surface, Surf. Sci., 307-309 (1994) 177-181.
[31] B. Hagman, A. Posada-Borbón, A. Schaefer, M. Shipilin, C. Zhang, L.R. Merte, A. Hellman, E. Lundgren, H. Grönbeck, J. Gustafson, Steps control the dissociation of CO_2 on Cu(100), J. Am. Chem. Soc., 140 (2018) 12974-12979.
[32] J. Neugebohren, D. Borodin, H.W. Hahn, J. Altschäffel, A. Kandratsenka, D.J. Auerbach, C.T. Campbell, D. Schwarzer, D.J. Harding, A.M. Wodtke, T.N. Kitsopoulos, Velocity-resolved kinetics of site-specific carbon monoxide oxidation on platinum surfaces, Nature, 558 (2018) 280-283.
[33] L. Zhou, A. Kandratsenka, C.T. Campbell, A.M. Wodtke, H. Guo, Origin of thermal and hyperthermal CO_2 from CO oxidation on Pt surfaces: The role of post-transition-state dynamics, active sites, and chemisorbed CO_2, Angew. Chem. Int. Ed., 58 (2019) 6916-6920.
[34] X. Liu, L. Sun, W.-Q. Deng, Theoretical investigation of CO_2 adsorption and dissociation on low index surfaces of transition metals, J. Phys. Chem. C, 122 (2018) 8306-8314.
[35] R. van Lent, S.V. Auras, K. Cao, A.J. Walsh, M.A. Gleeson, L.B.F. Juurlink, Site-specific reactivity of molecules with surface defects—the case of H_2 dissociation on Pt, Science, 363 (2019) 155-157.
[36] K. Cao, R. van Lent, A.W. Kleyn, M. Kurahashi, L.B.F. Juurlink, Steps on Pt stereodynamically filter sticking of O_2, Proc. Natl. Acad. Sci. U. S. A., (2019) 201902846.
[37] G. Kresse, J. Furthmuller, Efficient iterative schemes for ab initio total-energy calculations using plane wave basis set, Phys. Rev. B, 54 (1996) 11169-11186.
[38] G. Kresse, J. Furthmuller, Efficiency of ab initio total energy calculations for metals and semiconductors using plane wave basis set, Comp. Mater. Sci., 6 (1996) 15-50.

[39] J.P. Perdew, K. Burke, M. Ernzerhof, Generalized gradient approximation made simple, Phys. Rev. Lett., 77 (1996) 3865-3868.
[40] P.E. Blöchl, Projector augmented-wave method, Phys. Rev. B, 50 (1994) 17953-17979.
[41] H.J. Monkhorst, J.D. Pack, Special points for Brillouin-zone integrations, Phys. Rev. B, 13 (1976) 5188-5192.
[42] G. Henkelman, B.P. Uberuaga, H. Jónsson, A climbing image nudged elastic band method for finding saddle points and minimum energy paths, J. Chem. Phys., 113 (2000) 9901-9904.
[43] J. Ko, B.-K. Kim, J.W. Han, Density functional theory study for catalytic activation and dissociation of CO_2 on bimetallic alloy surfaces, J. Phys. Chem. C, 120 (2016) 3438-3447.
[44] B. Hammer, The NO+CO reaction catalyzed by flat, stepped, and edged Pd surfaces, J. Catal., 199 (2001) 171-176.
[45] S. Zhu, L. Guo, P. Li, B. Zhang, G. Zhao, T. He, A computational study on linear and bent adsorption of CO_2 on different surfaces for its photoreduction, Catal. Today, 335 (2019) 278-285.
[46] J.A. Gauthier, M. Fields, M. Bajdich, L.D. Chen, R.B. Sandberg, K. Chan, J.K. Nørskov, Facile Electron Transfer to CO2 during Adsorption at the Metal|Solution Interface, The Journal of Physical Chemistry C, 123 (2019) 29278-29283.
[47] A. Alavi, P. Hu, T. Deutsch, P.L. Silvestrelli, J. Hutter, CO oxidation on Pt(111): An ab initio density functional theory study, Phys. Rev. Lett., 80 (1998) 3650-3653.
[48] C.J. Zhang, P. Hu, A. Alavi, A density functional theory study of CO oxidation on Ru(0001) at low coverage, J. Chem. Phys., 112 (2000) 10564-10570.
[49] A. Eichler, CO oxidation on transition metal surfaces: reaction rates from first principles, Surf. Sci., 498 (2002) 314-320.
[50] X.-Q. Gong, R. Raval, P. Hu, CO dissociation and O removal on Co (0001): A density functional theory study, Surf. Sci., 562 (2004) 247-256.
[51] R. Alcalá, M. Mavrikakis, J.A. Dumesic, DFT studies for cleavage of C-C and C-O bonds in surface species derived from ethanol on Pt(111), J. Catal., 218 (2003) 178-190.
[52] P.J. Feibelman, B. Hammer, J.K. Nørskov, F. Wagner, M. Scheffler, R. Stumpf, R. Watwe, J. Dumesic, The CO/Pt(111) puzzle, J. Phys. Chem. B, 105 (2001) 4018-4025.[53] B.H. Peter J. Feibelman, J. K. Nørskov,F. Wagner, M. Scheffler, R. Stumpf, R. Watwe, J. Dumesic, The CO/Pt(111) Puzzle, The Journal of Chemical Physics B, 105 (2001) 4018-4025.